DISTRIBUTION STATEMENT A. Approved for public release; distribution is unlimited.

Remote Monitoring of Subsurface Flow Conditions in Rivers

Christopher J. Zappa
Lamont-Doherty Earth Observatory of Columbia University
Ocean and Climate Physics Division
61 Route 9W
Palisades, NY 10964
Phone: (845) 365-8547 fax: (845) 365-8157 email: zappa@ldeo.columbia.edu

Award Number : N00014-11-1-0922

LONG-TERM GOALS

The primary research goal is to develop techniques to determine subsurface turbulence from remote measurements using infrared imaging of the skin layer. We aim to infer flow rate, turbulence intensity and subsurface-generated turbulent structures from surface temperature patterns. We will take advantage of the two complementary indicators of subsurface flow provided by IR imagery: the thermal structures measured directly and the surface velocity fields obtained through various image processing techniques. We will (1) analyze the variability and structures of the thermal boundary layer, (2) compute the surface flow field from the IR imagery and infer further surface turbulence characteristics, (3) determine to which extent the turbulence in the boundary layer is due to surface forcing by analysis of the air-sea flux data and (4) determine empirical relationships of subsurface flow characteristics and of turbulence derived from in situ sub-surface data to the observed turbulence in the IR imagery. We further aim to determine the limits of remotely inferring flow rates, subsurface turbulence and bed stress from IR imagery. We will investigate how different wind, tides and wave breaking conditions affect our ability to remotely measure subsurface flow characteristics.

OBJECTIVES

The skin temperature is governed by surface and subsurface processes. Net air-water heat flux leads to a cooler thermal boundary layer (TBL) compared to the underlying bulk layer. Turbulent motions resulting from wind forcing at the air-sea interface and from turbulent eddies generated within the water column, disrupt the TBL, mixing it with the bulk layer. During the last century links between air-water transfer and bulk turbulence were researched [*Brumley and Jirka*, 1988; *Danckwerts*, 1951]. Only in the last decade, has the TBL been recognized as the intermediate step between subsurface turbulence and air-water transfer and as such was used as a more direct indicator for air-water transfer [*McKenna and McGillis*, 2004]. This study will use the TBL as a direct indicator for subsurface turbulence and provide predictive relationships of the surface-bulk connection. It will result in a be a set of universal curves connecting remotely collected surface measurements to fundamental local flow quantities – the flow depth, the bed stress, the bulk mean flow and the bulk turbulent kinetic energy.

APPROACH

Building on our extensive expertise in IR imagery and our experience in making near-boundary turbulence measurements, we aim to determine empirical relationships between surface length-scales and flow and sub-surface flow and turbulence. During the prototype field campaign, data was collected with the following instruments:

- IR camera: a Cedip Jade III longwave camera was mounted a pan/tilt system from the A-frame of a moored ship. This set up allowed us to move the camera with the current so to always view upstream of the ship. The Cedip Jade III offers better than 15 mK temperature resolution, with 200 Hz max frame rate, 14-bit digitization, and 320 x 240 pixels. The sampling frequency was set to 60 Hz.
- Air-Sea Flux package: a meteorological station was mounted on a piling neighbouring the ship to get measurements of wind speed & direction, relatively humidity, atmospheric pressure, air temperature, solar insolation, and longwave radiation.
- Acoustic Doppler Velocimeter (ADV): a Nortek Vector type ADV was mounted on the aforementioned piling at 11m above the River bed. Data was collected in 10 min bursts at top of every ½ hr, with a sampling frequency 32Hz.
- Higher Resolution Profilers: 2 Nortek Aquadopp were mounted on the piling at 3 and 6 m above the river bed. They offer a 1-cm resolution. Data was collected in 59.9 min burst at top of every hour, with a sampling frequency 2 Hz.
- CTDs: 3 CTDs were mounted on the piling at the same levels as the ADV and Aquadopps

The team's envisaged data analysis effort includes: image processing and analysis of the IR imagery to characterize surface turbulence. This comprises calculation of the statistical moments, histograms to assess surface skin temperature variability, and determination of length scales of the skin temperature structures. Further 3 methods to determine the surface velocity field from the IR imagery will allow inferring integral length scales, as well as the surface turbulent kinetic energy and calculation of divergence. The bulk Reynolds number can then be determined from the divergence. Analysis of the Aquadopps, ADV and CTD data combined will provide a robust measure of subsurface turbulent, convective, and advective motions. Links between the subsurface and surface turbulence will be investigated, keeping in mind that the observed turbulence at the surface is partly due to surface forcing. Processing and analysis of the direct measurement of heat, mass and momentum fluxes across the air-water interface along with measurements of the radiative forcing will permit to separate the different processes (wind-driven, bed-driven, buoyancy-driven, and convective) which lead to surface turbulence.

WORK COMPLETED

Our efforts FY14 comprised image processing and analysis of IR imagery taken from the ship and analysis of in situ measurmeents so to address points (1) through (4) of the long term goals. Skin temperature variance was shown to decrease with increasing wind speend and latent heat flux. Surface integral length scales were determined from the skin temperature and are shown to be linearly related to water column depth. Surface currents were derived via three algorithms: Digital Particle Image Velocimetry, Optical Flow and Spectral Advective Surface. They gave estimates that were highly

correlated to the subsurface flow measurements with comparable 10 minute mean magnitudes. We have presented our results at the AGU Fall Meeting, San Francisco, CA, USA in December 2011 [*Zuckerman et al.*, 2011] and 2012 [*Brumer et al.*, 2012]. We have two manucripts that are in preparation to be submitted. One describes the characteristic surface length scale determined from IR imagery and its relatinoship to water depth. A second manucript is on skin temperature variability response to surface turbulence and heat flux.

RESULTS

Surface Current Retrievals Validation

We will simultaneously use 3 approaches to determine surface velocity fields:

1. Feature tracking or Digital Particle Image Velocimetry (DPIV; e.g. *McKenna and McGillis* [2002], *Variano and Cowen* [2008])
2. Optical flow (OF; e.g., *Lucas and Kanade* [1981])
3. Spectral Advective Surface (SAS) in 3D spectra of the skin temperature [*Dugan and Piotrowski*, 2012]

to investigate both the bulk flow (which we wish to parameterize) and the near-surface region (where the physics responsible for translating bulk motions into surface motions occurs). The surface flow estimates from the different algorithms correlate well as depicted in Figure 1 Left where the run mean flow magnitudes are compared. Strongest correlation exists between the SAS method and the DPIV, with r^2=0.96.

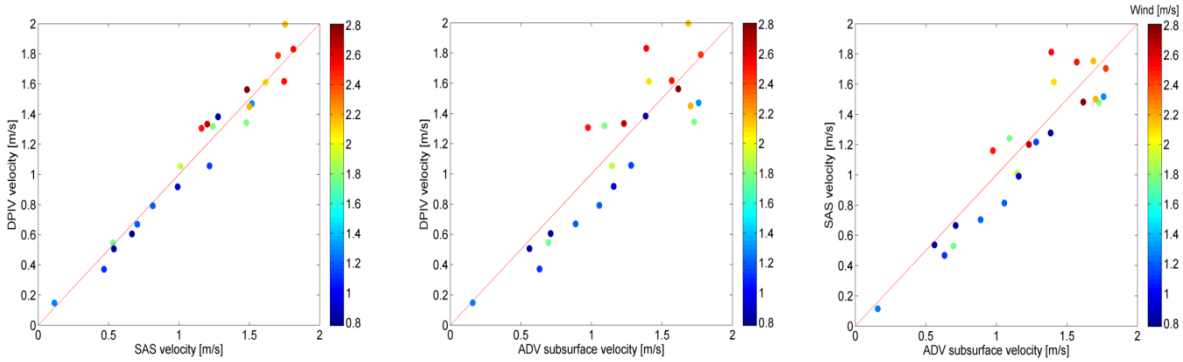

Figure 1. (Left) Scatter plot of the run mean flow magnitudes derived from the DPIV method against those of the SAS method. The red line denotes the 1:1 correlation. Scatter plots of the run mean flow magnitude of the measured and imagery derived flow magnitudes for (Middle) DPIV vs. ADV and for (Right) SAS vs. ADV.

Comparing the magnitudes of the velocities derived from the skin temperature with the 3 different methods to those measured by the ADV, we see good agreement between the measured and the IR derived velocities (c.f. Figure 1 Middle/Right). The correlation coefficients between the ADV measured velocity magnitudes are high: r^2 = 0.80 for the DPIV, r^2 = 0.79 for the OF, and r^2 = 0.87 for the SAS flow magnitudes. Taking the top good bin of the ADCP, which is at around ~0.4 m depth, the surface derived velocity are again compared to in situ giving r^2 = 0.88, r^2 = 0.82, and r^2 = 0.92 for

DPIV, OF and SAS estimates respectively. The ADCP current measurements at the height of the ADV correlate with the ADV measurement at $r^2 = 0.88$.

Correlation coefficients do not provide sufficient information to conclude on how imagery derived flows compare to measured subsurface flows as it only provides an insight on how closely they are linearly related, but says nothing about how they compare in actual magnitude. The scatter plots (c.f. Figure 1 Middle/Right) clearly show that not only are they well correlated, but they are also of comparable magnitude.

Characteristic Surface Length Scale

(a)

(b)

(c)

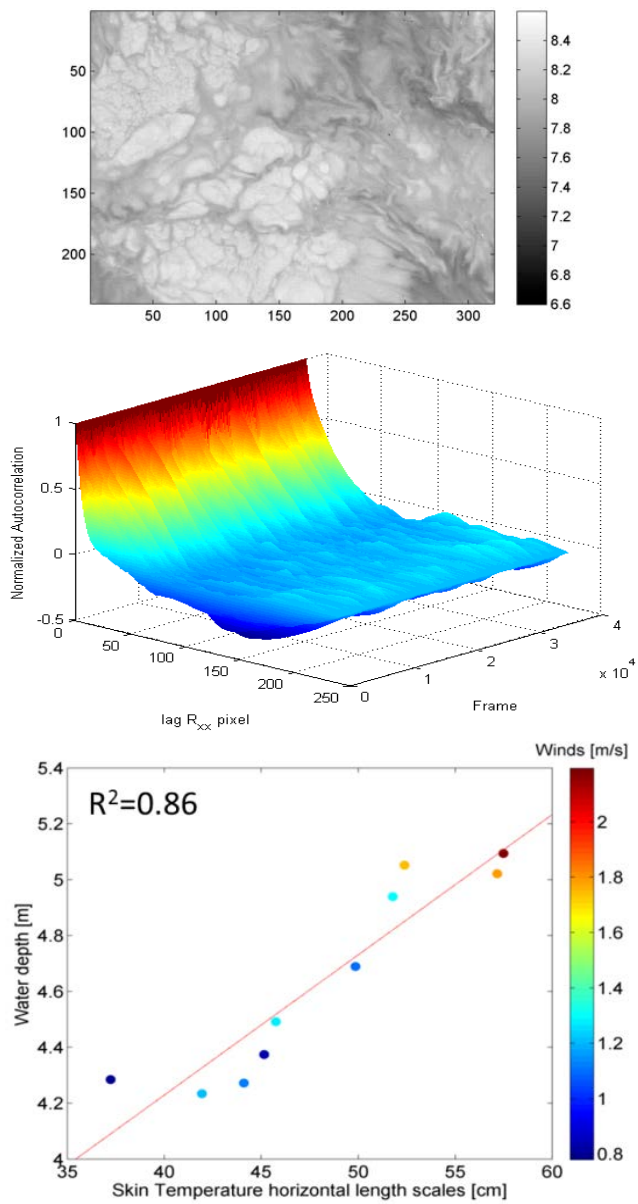

Figure 2. (a) Sample calibrated thermal image; (b) Sample timeseries of the frame averaged normalized spatial autocorrelation of the thermal imagery for various lags. (c) Scatter plot of the surface scales derived from the spatial autocorrelation functions against height of the water column

Figure 2a shows a typical infrared image of the Hudson River surface at the scale of roughly 2.5m by 3.0m. In order to determine the characteristic surface length scale we computed a normalized auto-covariance function for each row and column of each frame (an example of which is shown in Figure 2b). Then a frame mean normalized auto-covariance function was computed by averaging these over rows and columns. The characteristic integral length scale was determined as the distance at which the temperatures are no longer correlated, i.e. corresponding to the smallest lag at which the frame mean auto-covariance function is equal to zero. Figure 3c shows a scatter plot of the integral length scales derived from the skin temperature fields versus water depth. It suggests the scale of the surface features (δ) is strongly linearly correlated (r^2=0.86) to the water depth (D), with a slope of $D/\delta \sim 9.5$. This demonstrates the capability to provide quantitative spatial and temporal properties of the mean flow and coherent structures to be compared to the subsurface turbulent properties.

The first hypothesis that comes to mind as to the physical explanation of the relation between surface scales and depth, is that the size of the boils that come up to the surface disrupting the TBL, increases with the water column depth. This hypothesis is supported by the work of *Korchoka* [1968] and *Jackson* [1976] who found that the size of boils coming up to the surface is proportional to the water column depth. *Jackson* [1976] plotted the boil diameter (*Ø*) against the water depth (*d*) measured by *Korchoka* [1968] in the Polomet River in Russia and showed that they correlate well within a band delimited by the two lines: *d/ Ø=1.75* and *d/ Ø=3.7.* These slopes are much smaller than the one we observed in this study. This could maybe be explained by the different origin of the signal observed. Here, the temperature signal is detected, whereas *Jackson* [1976] used visual observations for his estimates. The relation between boil diameter and flow depth may be expected from the scaling relation proposed by *Rao et al.* [1971], relating the boundary layer thickness (δ) to the free stream velocity (U_∞) and a mean periodicity of bursting: $U_\infty T/\delta \approx 5$, where $U_\infty \bar{T}$ defines a turbulence length scale [*Tennekes and Lumley*, 1972]. Combining data from the Polomet and Wabash rivers, *Jackson* [1976] found that on average $U_\infty T/\delta \approx 7.6$, which is closer to the slope we calculated.

TKE Dissipation

The turbulent kinetic energy (TKE) dissipation rate ϵ can be estimated by fitting the inertial subrange of wavenumber spectra ($\Phi(k)$) with a $k^{-5/3}$ slope following the Kolmogorov turbulence cascades which dictates that:

$$\Phi(k) = \alpha \epsilon^{\frac{2}{3}} k^{-\frac{5}{3}}$$

where k denotes the wavenumber and α is a constant. Wavenumber spectra can be computed directly from the IR derived velocity fields or Aquadopp profiles. However, for time series measurement of velocities such as collected by ADVs, it is necessary to make a further assumption in order to derive TKE dissipation rates. Assuming that the frozen Taylor hypothesis is valid, i.e. that turbulent eddies remain unchanged while being advected by the mean flow, one can convert frequency spectra $S(f)$ into wavenumber spectra as follows:

$$\Phi(k) = S(f).\frac{\langle v \rangle}{2\pi}, \text{ with } k = 2\pi f/\langle v \rangle$$

where f is the frequency and $\langle v \rangle$ the mean velocity.

Surface derived TKE dissipation rates match the subsurface dissipations well (c.f. Figure 3). However, the correlation is worse when the Taylor Hypothesis had to be employed for the subsurface, giving significantly lower correlations (r^2=0.35) between the DPIV and ADV derived dissipation rates. The correlation is high (r^2=0.8) when the dissipation is calculated directly from wavenumber spectra, even

when compared to the bottom instruments. The strong correlation throughout the water column is to be expected from the low shear and stratification.

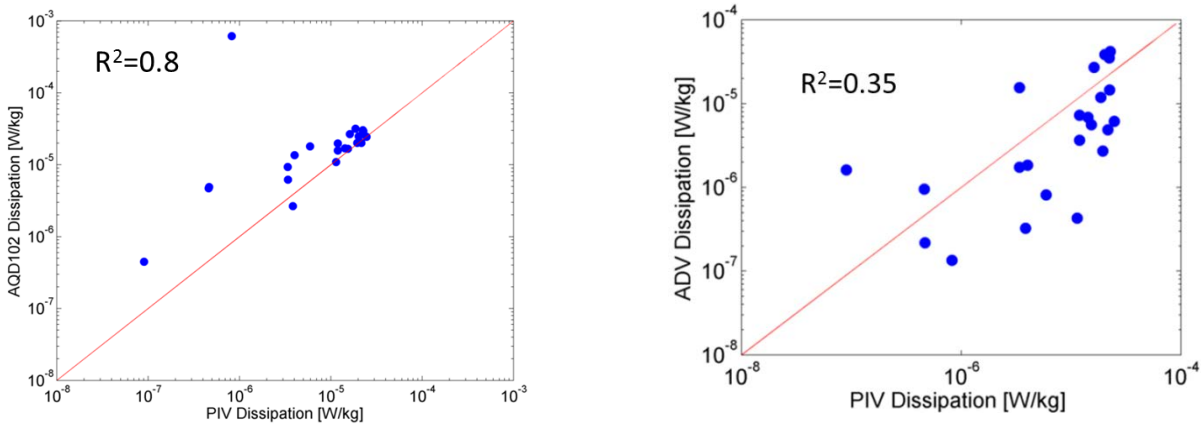

Figure3. DPIV derived TKE dissipation rates versus (left) that from the Bottom Aquadopp at 1.83 m above the river bed and (right) that from the ADV at 3.35 m above the river bed

Skin Temperature Variability Response to Surface Turbulence and Heat Flux

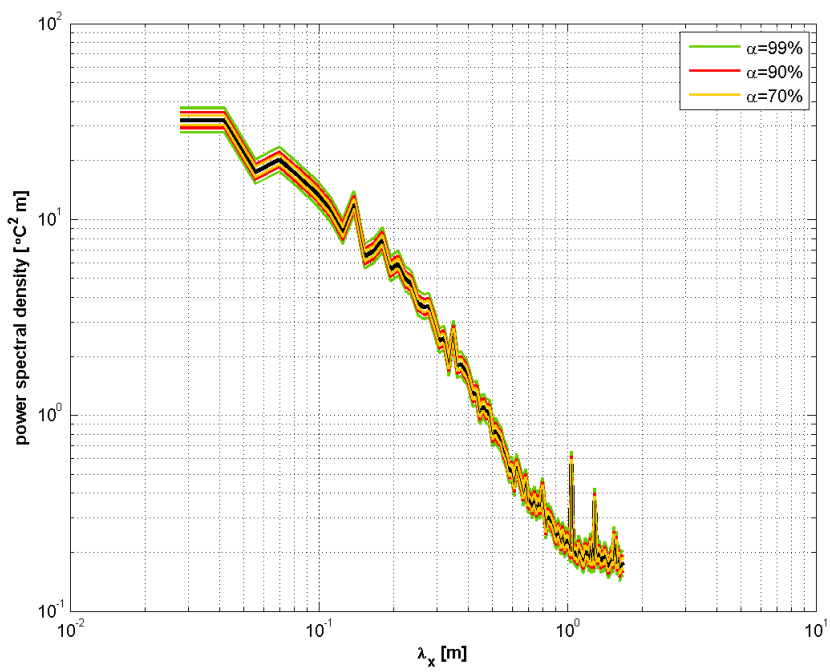

Figure 4. Example of a mean wavenumber spectrum of calibrated skin temperature from the Hudson River IR data (black line). The colored lines delimit the confidence interval for different confidence level.

The capabilities provided by our Hudson River data set acquired from an IR camera mounted on a

barge on the river combined with that of the IR imagery from the Palisade Cliff-Side Lookout provided by Areté Associates allow us to determine the spatio-temporal surface temperature structure from scales of *O*(0.01 to 1000)m, or 5 orders of magnitude. The classic wavenumber spectra of surface skin temperature shown in Figure 4 characterizes the smallest scales relevant to turbulent boundary layers in nature.

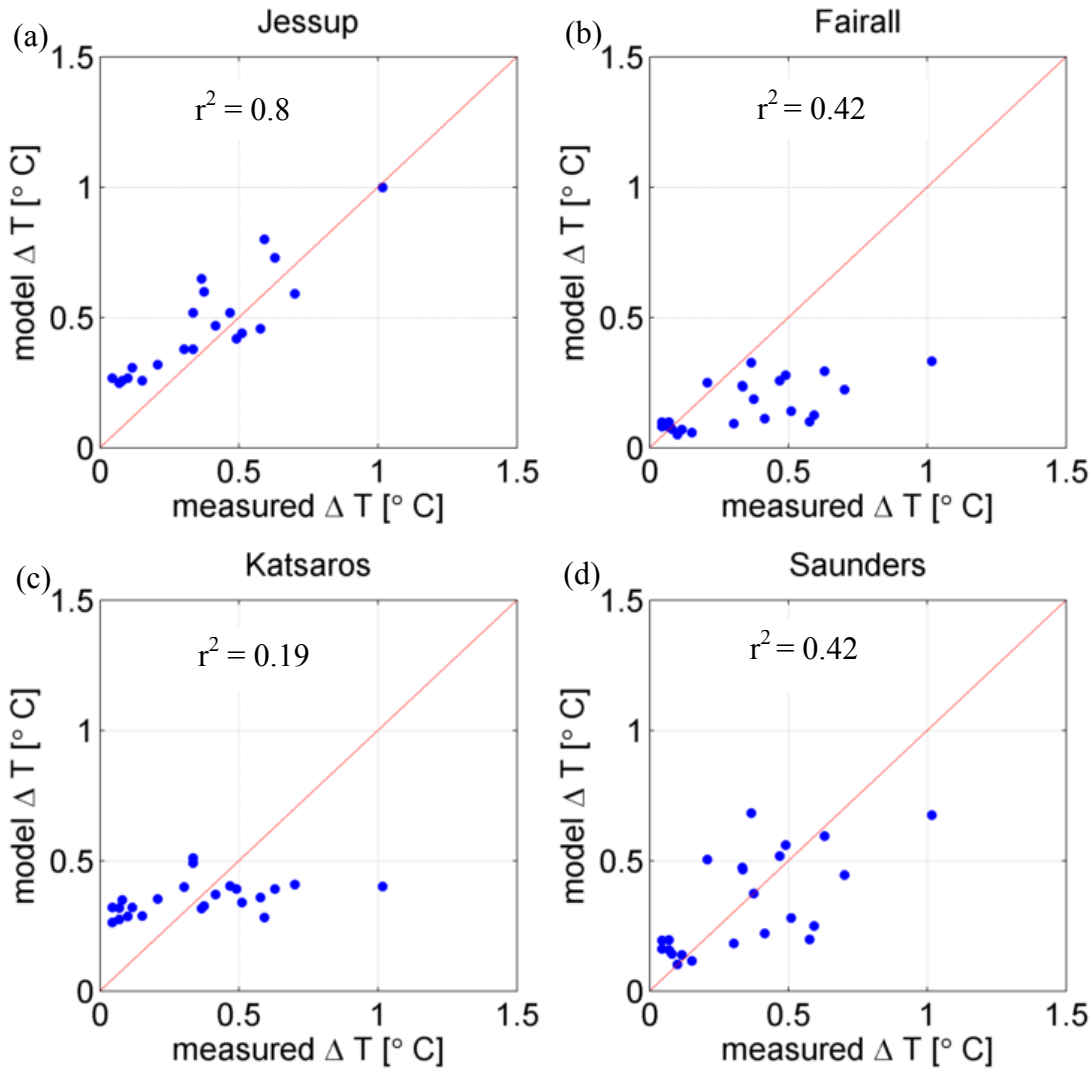

Figure 5. Scatter plots of modeled bulk-skin temperature difference (ΔT) against measured ΔT. The measured ΔT was calculated from CTD and IR measurements. The model ΔT is based (a) on Jessup et al. [2009], (b) Fairall et al. [1996], (c) Katsaros et al. [1977], and (d) Saunders [1967].

We have evaluated the validity of several bulk-skin temperature (ΔT) models found in the literature (c.f. *Figure 5*). The first set of models tested were those based on the probability distribution of the skin temperature as obtained from IR imagery ($p(T_{skin})$). *Jessup et al.* [2009] determined ΔT purely from IR imagery, taking the 99 percentile temperature as the bulk temperature. This assumes

complete renewal of the surface and was found to most accurately represent the measured ΔT. *Garbe et al.* [2004] assumed that $p(T_{skin})$ follows a log-normal distribution. This model was found to be inadequate as most $p(T_{skin})$ derived from our IR imagery did not display the assumed distribution. Indeed, most $p(T_{skin})$ were Gaussian looking and some clearly were bimodal. Another group of models tested were those based on the assumption that heat transfer across the skin layer occurs through molecular conduction (k), implying $\Delta T = \lambda * Q\delta/k$, where Q is the net heat flux, δ is the thickness of the thermal boundary layer and λ a proportionality factor . *Saunders* [1967] determined δ assuming a forced convection regime whereas *Katsaros et al.* [1977] model assumes free convection. *Fairall et al.* [1996] allows for a transition between free and forced convection. Katsaros' model does not represent the spread in ΔTs observed suggesting that the data was taken during a forced rather than free convection regime which corroborates with the better fit of Saunders' model. Saunders' lambda was found to be 11.87, which is within the range found in the literature. Fairall's lambda which accounts for shear and buoyancy effects was computed to be ~5.9 which appears to be too small to fit the measured ΔT.

Skin Temperature Variability Response to Wind Gustiness

During windier nights such as Nov 19th, sporadic gust events can be seen in the large scale IR imagery taken from the cliff mounted camera. These are characterized by brighter patches or fronts propagating through the images at higher speed than the surrounding features. We have successfully matched times of gust events passing over the pilling with peaks in wind measured by the anemometer on the pilling (c.f. Figure 6). Increased brightness under gusts may be due either to warming of the skin or increased roughness. Warming of the skin could be due to a disruption in the thermal boundary layer leading to a decreased bulk-skin temperature difference or reflect a pure skin layer response due to enhanced heat flux. Changes in surface roughness can also change the emissivity at high incidence angles. A partly cloudy sky would explain an increased brightness under increased roughness conditions. Gustiness can also increase the local heat flux and the change the temperature gradient across surface thermal boundary layer. All may impact the IR signature due to gustiness. We will explore whether the gust signal seen in the IR imagery is an optical/electromagnetic signal and/or reflects processes in the thermal boundary. This will be done by identifying signatures of the gust in the calibrated small scale imagery recorded from the barge.

Preliminary analysis suggests that often there is a lag between the wind peak and the IR signal, with the peak in winds occurring before the gust is seen to reach the instrument piling. Such a lag is to be expected if the gust signal seen in the IR imagery is an optical/electromagnetic rather than thermal signature as waves resulting from the gust take time to grow, whereas temperature would respond quicker.

Figure 7(a-c) shows an example of a gust passing over the field of view of the IR camera mounted on the barge. On the leading edge of the gust, a darker, colder front is seen in the cliff based imagery followed by a brighter, warmer patch. This corresponds to a sharp decreased followed by an equally sharp increase in skin temperature measured by the barge IR imager (c.f. Figure 7 d & e). Warming is observed for only a portion of the gust events detected in the cliff imagery. This hints to the fact that both warming and increased roughness. Cliff and ship based cameras were mounted at different grazing angles. Roughness induced gust signatures in the large scale image may not be detectable in small scale imagery. More extensive analysis of the small scale imagery will give us an insight of the physical effects of gusts.

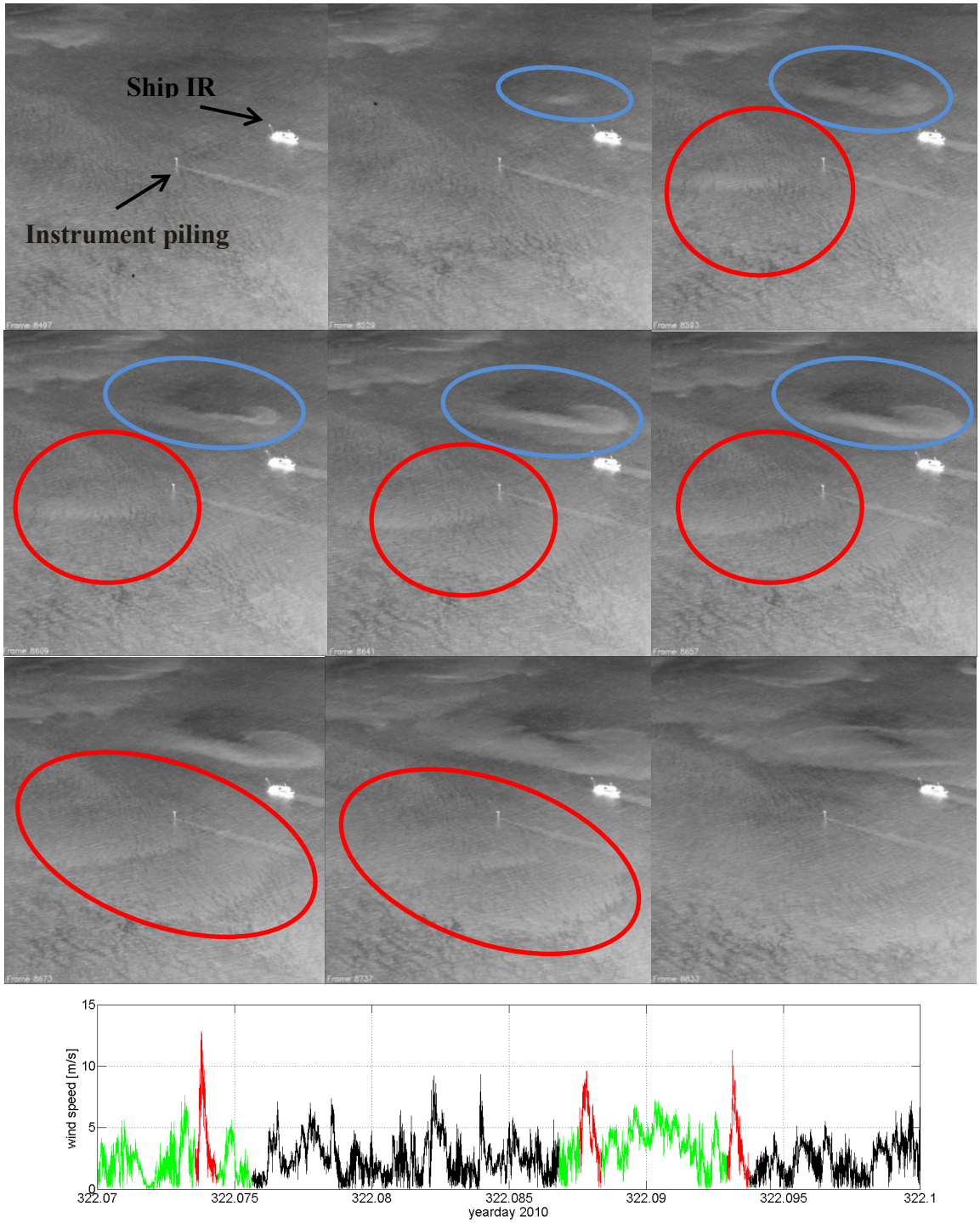

Figure 6. (a) Infrared imagery taken from the cliff in which two gust events can be seen, demarked by the blue and red shapes. The gust circled in red passes over the instrument pilling. This event corresponds to the first red peak in the wind time series below. (b) Time series of wind speed measured at the piling; in green the period of time during which cliff imagery was recorded, in red, the periods corresponding to gusts events as detected in the cliff imagery

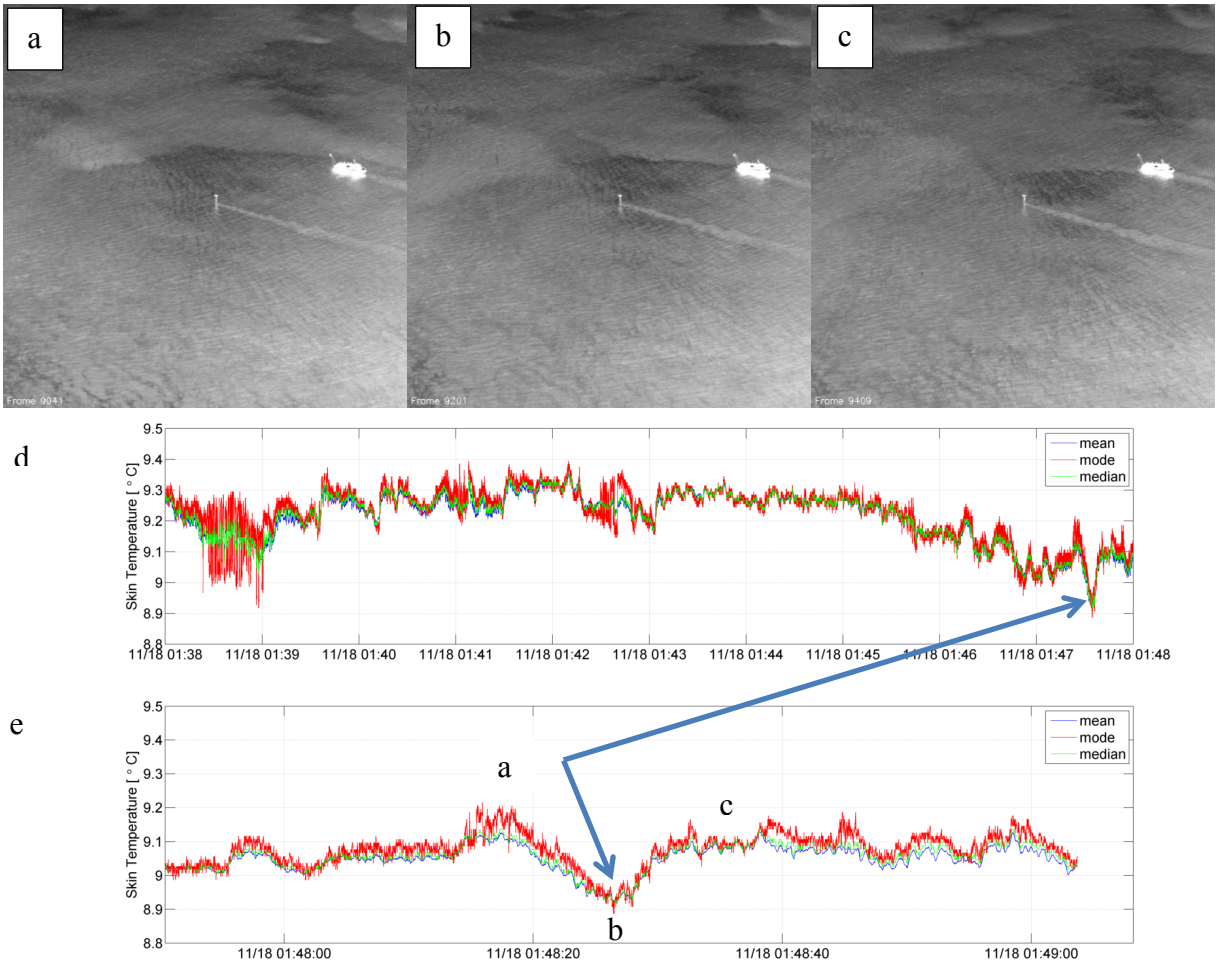

Figure 7. (a), (b) and (c) sequence of cliff based IR imagery showing the propagation of a gust over the barge. (d) 10 minute time series of skin temperature determine from the calibrated barge imager. The gust event described in (a), (b) and (c) occurred at the end of the run when the skin temperature in seen to sharply decrease then increase; time identified by the blue arrow. (e) blow up of (d) around the time of the gust event; letters (a), (b) and (c) indicate the time at which the cliff snapshots were taken.

IMPACT/APPLICATIONS

Although in this field campaign the IR remote sensing was performed from a ship, the analysis and results obtained in this study should be easily adaptable to imagery taken from other platforms such as aircrafts, manned and unmanned, as well as fixed platforms. This study reinforces the idea that IR remote sensing is an excellent surveying tool for estuarine environments and encourages continued research in the field. The strong linear relation between depth and surface integral length scales derived from the temperature fields may provide a useful method to estimate bathymetry, especially when no waves are present.

The good agreement between the IR derived and sub-surface TKE dissipation estimates reinforces the adequacy of IR remote sensing for studies of estuarine and riverine turbulence. Previous studies have already shown how IR derived dissipation rates reflects in situ measured dissipation well [e.g.,

Chickadel et al., 2011]. Unlike us, they made use of the Taylor hypothesis even for the imagery estimates, choosing to compute dissipation at a single location. Our results strongly suggest that not having to assume the validity of the Taylor hypothesis gives significantly better results.

REFERENCES

Brumer, S. E., C. J. Zappa, S. P. Anderson, and J. P. Dugan (2012), Using skin temperature variability to quantify surface and subsurface estuarine processes, *AGU Fall Meeting Abstracts*, *14*, 05.

Brumley, B. H., and G. H. Jirka (1988), Air-water transfer of slightly soluble gases: Turbulence, interfacial processes and conceptual models, *PhysicoChemical Hydrodynamics*, *10*(3), 295-319.

Chickadel, C. C., S. A. Talke, A. R. Horner-Devine, and A. T. Jessup (2011), Infrared-based measurements of velocity, turbulent kinetic energy, and dissipation at the water surface in a tidal river, *IEEE Geoscience and Remote Sensing Letters*, *8*(5), 849-853, doi:10.1109/LGRS.2011.2125942.

Danckwerts, P. V. (1951), Significance of liquid-film coefficients in gas absorption, *Industrial and Engineering Chemistry*, *43*(6), 1460-1467.

Dugan, J. P., and C. C. Piotrowski (2012), Measuring currents in a coastal inlet by advection of turbulent eddies in airborne optical imagery, *J. Geophys. Res.*, *117*(C03020), doi:10.1029/2011JC007600.

Fairall, C. W., E. F. Bradley, J. S. Godfrey, G. A. Wick, J. B. Edson, and G. S. Young (1996), Cool-skin and warm-layer effects on sea surface temperature, *J. Geophys. Res.*, *101*(C1), 1295-1308.

Garbe, C. S., U. Schimpf, and B. Jähne (2004), A surface renewal model to analyze infrared image sequences of the ocean surface for the study of air-sea heat and gas exchange, *J. Geophys. Res.*, *109*(C08S15), doi:10.1029/2003JC001802.

Jackson, R. G. (1976), Sedimentological and fluid-dynamic implications of the turbulent bursting phenomenon in geophysical flows, *Journal of Fluid Mechanics*, *77*(03), 531-560.

Jessup, A. T., W. E. Asher, M. Atmane, K. Phadnis, C. J. Zappa, and M. R. Loewen (2009), Evidence for complete and partial surface renewal at an air-water interface, *Geophys. Res. Lett.*, *36*(L16601), doi:10.1029/2009GL038986.

Katsaros, K. B., W. T. Liu, J. A. Businger, and J. E. Tillman (1977), Heat transport and thermal structure in the interfacial boundary layer measured in an open tank of water in turbulent free convection, *Journal of Fluid Mechanics*, *83*(2), 311-335.

Korchoka, Y. (1968), Investigation of the dune movement of sediments on the Polomet River, *River. Sov. Hydrol*, 541-559.

Lucas, B. D., and T. Kanade (1981), An Iterative Image Registration Technique with an Application to Stereo Vision, *Proceedings of Imaging Understanding Workshop*, 121-130.

McKenna, S. P., and W. R. McGillis (2002), Performance of digital image velocimetry processing techniques, *Exp. Fluids*, *32*, 116-115, doi:DOI 10.1007/S003480100348.

McKenna, S. P., and W. R. McGillis (2004), The role of free-surface turbulence and surfactants in air-water gas transfer, *International Journal of Heat and Mass Transfer*, *47*, 539-553.

Rao, K. N., R. Narasimha, and M. Narayanan (1971), The 'bursting'phenomenon in a turbulent boundary layer, *Journal of Fluid Mechanics*, *48*(02), 339-352.

Saunders, P. M. (1967), The temperature at the ocean-air interface, *Journal of the Atmospheric Sciences*, *24*, 269-273.

Tennekes, H., and J. L. Lumley (1972), *A First Course in Turbulence*, MIT Press, Cambridge, Mass.

Variano, E. A., and E. A. Cowen (2008), A random-jet-stirred turbulence tank, *Journal of Fluid Mechanics*, *604*, 1-32, doi:10.1017/S0022112008000645.

Zuckerman, S., S. P. Anderson, C. J. Zappa, and R. A. Smith (2011), Infrared Observations of Temperature Modulations on the Hudson River, *AGU Fall Meeting Abstracts*, *51*, 1331.

PUBLICATIONS

Brumer, S. E., C. J. Zappa, S. P. Anderson, and J. P. Dugan (2012), Using skin temperature variability to quantify surface and subsurface estuarine processes, *AGU Fall Meeting Abstracts*, *14*, 05. [Published].

Zuckerman, S., S. P. Anderson, C. J. Zappa, and R. A. Smith (2011), Infrared Observations of Temperature Modulations on the Hudson River, *AGU Fall Meeting Abstracts*, *51*, 1331. [Published].